Opposite Effects of High-Valent Cations on the Elasticities of DNA and RNA Duplexes Revealed by Magnetic Tweezers

Hang Fu,[1,*] Chen Zhang,[1,*] Xiao-Wei Qiang,[2,*] Ya-Jun Yang,[1] Liang Dai,[3] Zhi-Jie Tan,[2,‡] and Xing-Hua Zhang[1,†]

[1]College of Life Sciences, the Institute for Advanced Studies, State Key Laboratory of Virology, Hubei Key Laboratory of Cell Homeostasis, Wuhan University, Wuhan 430072, China

[2]Center for Theoretical Physics and Key Laboratory of Artificial Micro & Nano-structures of Ministry of Education, School of Physics and Technology, Wuhan University, Wuhan 430072, China

[3]Department of Physics, City University of Hong Kong, Hong Kong 999077, China

(Received 8 May 2019; accepted 16 January 2020; published 7 February 2020)

We report that trivalent cobalt hexammine cations decrease the persistence length, stretching modulus, helical density, and size of plectonemes formed under torque of DNA but increase those of RNA. Divalent magnesium cations, however, decrease the persistence lengths, contour lengths, and sizes of plectonemes while increasing the helical densities of both DNA and RNA. The experimental results are explained by different binding modes of the cations on DNA and RNA in our all-atom molecular dynamics simulations. The significant variations of the helical densities and structures of DNA and RNA duplexes induced by high-valent cations may affect interactions of the duplexes with proteins.

DOI: 10.1103/PhysRevLett.124.058101

In vertebrate spermatozoa, highly negatively charged double-stranded (ds) DNA is packed into toroids mediated by cationic proteins and high-valent (≥3) cations. The dsDNA can be effectively condensed by high-valent cations whereas its closest cousin dsRNA resists condensation [1]. To understand this contradiction, extensive studies have been performed on different effects of high-valent cations on physical properties of dsDNA and dsRNA [2–5]. Recent simulations have predicted that $CoHex^{3+}$ and $spermine^{4+}$ decrease the bending persistence length (P) of dsDNA but increase that of dsRNA [6]. To confirm and further elaborate these simulation results by experiments in this work, we use $CoHex^{3+}$ as a representative high-valent cation. In addition, we choose Mg^{2+} as a control, because Mg^{2+} cannot condense DNA.

The effects of cations on the tensile elasticities of dsDNA and dsRNA have been measured by single-molecule experiments. Monovalent salts decrease P_{DNA} and P_{RNA} through the screening of the electrostatic repulsions between the negative charges on the DNA backbone [7–15]. Similarly, divalent cations decrease P_{DNA} [10,15–17]. High-valent cations decrease P_{DNA} [16–18] and highly cationic agents condense DNA [18–29]. Currently, there are little experiments for the effects of multivalent (≥2) cations on the tensile elasticities of dsRNA. How cations affect the helical structures of dsDNA and dsRNA is still unclear.

In this work, we characterized the elasticities of dsDNA and dsRNA using magnetic tweezers (MT) [Fig. 1(a)] [14]. We determined the tensile elasticities using the end-opened (torsion-free) DNA and RNA and determined the torsional elasticities using the torsion-constrained constructs [Fig. 1(b)]. We prepared the torsion-constrained RNA by a universal assay to make DNA, RNA, and RNA-DNA hybrid configurations [30], and acquired all data at 1 mM Tris-HCl pH 7.5 and 20 °C. Details about the preparation of the DNA and RNA constructs and elasticity measurements can be found in the Supplemental Material [31] (Fig. S1) and the previous works by others [35] and by us [14,30,36–38].

First, we determined the effects of multivalent cations on the tensile elasticities of dsDNA and dsRNA through measurements of the force-extension (F-x) curves [Figs. 2(a) and 2(b)]. We fitted each F-x curve to an approximation formula for the extensible wormlike chain model (black line) [39]:

$$\frac{x}{NL} = 1 - \sqrt{\frac{k_B T}{4FP}} + \frac{F}{K}. \tag{1}$$

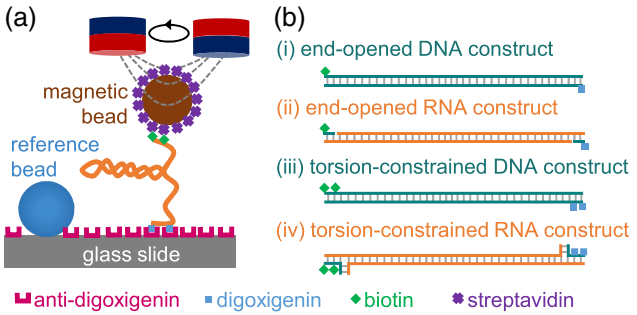

FIG. 1. Experimental setup. (a) The home-built MT. A pair of NdFeB magnets is used to stretch and twist the molecule anchored between a glass slide and a microbead. (b) Four DNA and RNA constructs with the same sequences (19 116–31 647 bp of lambda DNA, 43.3% GC content).

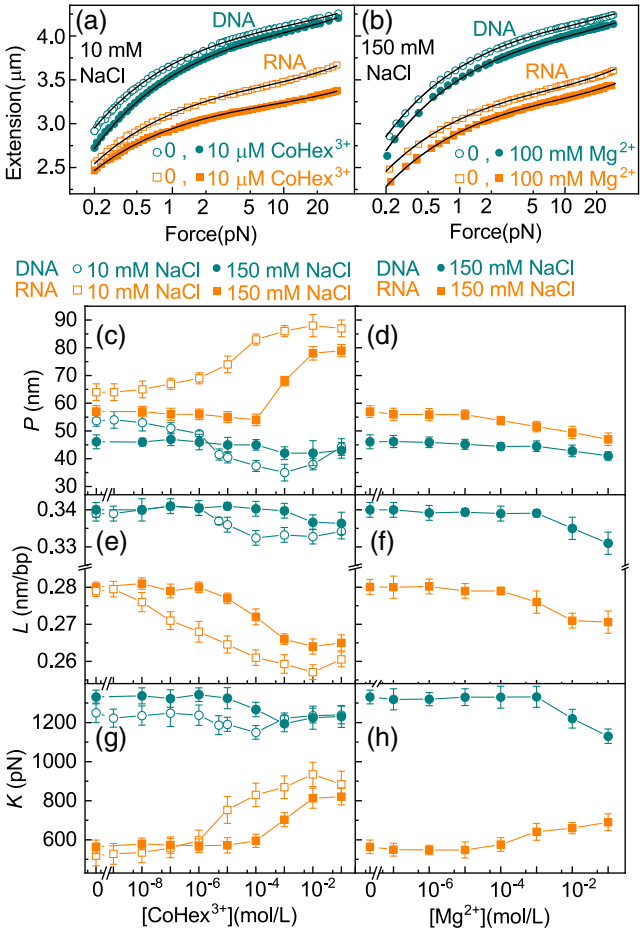

FIG. 2. Effects of $CoHex^{3+}$ and Mg^{2+} on the tensile elasticities of the dsDNA and dsRNA. (a)–(b) Representative F-x curves. Each F-x curve is fitted to Eq. (1) (black line), yielding P, L, and K. (c)–(h) The average and SEM of P, L, and K obtained from more than four molecules are plotted as data points and error bars.

Here, the two measured variables x is the extension of the molecule and F is the force. The fitting parameters L is the contour length per base pair, and K is the stretching modulus. $N = 12\,531$ is the number of base pairs. Although Eq. (1) is not rigorous, it is simple, precise, and has been widely used to analyze the experimental F-x curves of dsDNA and dsRNA [12,14,16–18,37,38].

Figure 2(c) shows that in the presence of 10 mM NaCl, $CoHex^{3+}$ significantly decreases P_{DNA} from 54 ± 2 to 35 ± 3 nm until 1 mM $CoHex^{3+}$, which agrees with previous single-molecule results [16–18]. It is interesting that the trend of P_{DNA} reverses beyond 1 mM $CoHex^{3}$, which may be due to the charge inversion of DNA caused by excessive binding of $CoHex^{3+}$ to the DNA backbone since the P-reversion $CoHex^{3+}$ concentration is near the charge-reversion $CoHex^{3+}$ concentration of DNA at a similar monosalt concentration [25]. Different from the case of DNA, $CoHex^{3+}$ monotonically increases P_{RNA} at 10 mM NaCl (64 ± 3 to 87 ± 3 nm), which confirms the simulation results that $CoHex^{3+}$ affects P_{DNA} and P_{RNA} oppositely [6]. At 150 mM NaCl, $CoHex^{3+}$ affects P_{DNA} and P_{RNA} oppositely as well but higher $CoHex^{3+}$ concentration is required than at 10 mM NaCl, which may be due to competitive binding of Na^{+} and $CoHex^{3+}$.

As shown in Fig. 2(e), $CoHex^{3+}$ (0–100 mM) slightly shortens L_{DNA} (0.339 ± 0.002 to 0.334 ± 0.002 nm/bp) whereas it significantly shortens L_{RNA} (0.279 ± 0.002 to 0.260 ± 0.002 nm/bp) at 10 mM NaCl, which confirms the recent simulations as well [6]. At 150 mM NaCl, the shortening in both L_{DNA} and L_{RNA} occurs at higher $CoHex^{3+}$ concentrations.

We found $CoHex^{3+}$ affects the K of DNA and RNA oppositely [Fig. 2(g)]. At 10 mM NaCl, $CoHex^{3+}$ moderately reduces K_{DNA} from 1250 ± 50 to 1150 ± 35 pN until the trend reversion at 100 μM $CoHex^{3+}$. Opposite to the case of DNA, $CoHex^{3+}$ monotonically raises K_{RNA} from 519 ± 52 to 884 ± 67 pN until 100 mM $CoHex^{3+}$. At 150 mM NaCl, $CoHex^{3+}$ affects K_{DNA} and K_{RNA} oppositely as well, but a higher $CoHex^{3+}$ concentration is required than in the case of 10 mM NaCl.

As a negative control for $CoHex^{3+}$, we measured the effects of Mg^{2+} on F-x curves of dsDNA and dsRNA at 150 mM NaCl [Fig. 2(b)]. Mg^{2+} decreases both P_{DNA} and L_{RNA} until 100 mM [Figs. 2(d) and 2(f)]. Until 100 mM, Mg^{2+} reduces K_{DNA} but raises K_{RNA} [Fig. 2(h)].

In addition to the tensile elasticities, we determined the effects of multivalent cations on the torsional elasticities of dsDNA and dsRNA by measuring the rotation-extension (R-x) curves at 0.3 pN [Figs. 3(a) and 3(b)]. For each R-x curve, starting from the torsion-relaxed point, the first of a few rotations decreases the molecule extension slowly. Beyond the critical buckling point, further rotations decrease the molecule extension rapidly and linearly, which is attributed to the formation of plectonemes under torque [13,40,41]. The R-x curves are shifted by multivalent cations while maintaining the bell-like shape. We also plot the molecule extension normalized by total contour length ($x/L/N$) as a function of the external rotation normalized by the total helical number ($\Delta\sigma_e$) [Figs. 3(c) and 3(d)]. More representative R-x curves are shown in Fig. S2 [31].

It is possible that condensation or some other chain-chain interactions at high $CoHex^{3+}$ concentrations distort R-x curves and then affect the extraction of torsional elasticities (Fig. S2d [31]) [26]. Thus, we only calculated the torsional elasticities at low $CoHex^{3+}$ concentrations where the R-x curves are not distorted. The relative change in the helical density induced by multivalent cations ($\Delta\sigma$) is determined to be the shift in the torsion-relaxed point divided by total helical numbers of the duplex [arrows, Figs. 3(c) and 3(d)]. The size of plectonemes (δ) is determined to be the slope of extension decreased with rotations in the plectoneme region upon overwinding [black lines, Figs. 3(a) and 3(b)] [13,40].

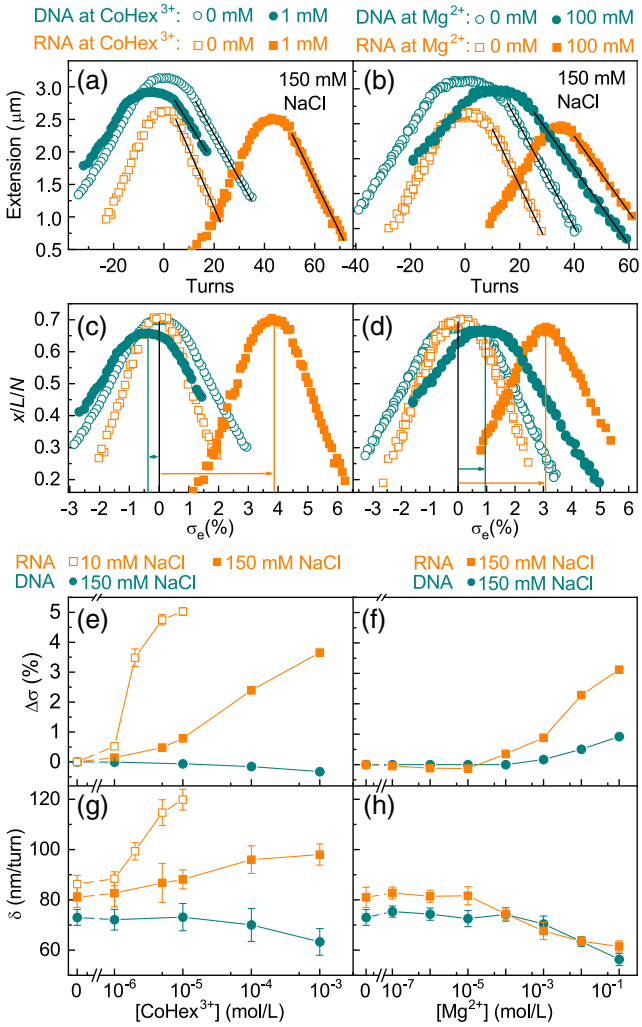

FIG. 3. Effects of $CoHex^{3+}$ and Mg^{2+} on the torsional elasticities of dsDNA and dsRNA. (a)–(b) Representative R-x curves where condensation is absent. (c)–(d) R-x curves in dimensionless variables. (e)–(h) The average and SEM of $\Delta\sigma$ and δ obtained from more than four molecules are plotted as data points and error bars. Some error bars are smaller than the symbols, which are invisible.

$CoHex^{3+}$ affects the torsional elasticities ($\Delta\sigma$ and δ) of dsDNA and dsRNA oppositely. As shown in Fig. 3(e), 1 mM $CoHex^{3+}$ slightly underwinds DNA by $0.32 \pm 0.01\%$ but significantly overwinds RNA by up to $3.66 \pm 0.10\%$ at 150 mM NaCl. At 10 mM NaCl, 10 μM $CoHex^{3+}$ further overwinds RNA by up to $5.03 \pm 0.13\%$. As shown in Fig. 3(g), 1 mM $CoHex^{3+}$ decreases δ_{DNA} from 73 ± 3 to 63 ± 5 nm/turn but increases δ_{RNA} from 81 ± 4 to 98 ± 4 nm/turn at 150 mM NaCl. At 10 mM NaCl, 10 μM $CoHex^{3+}$ further increases δ_{RNA} from 86 ± 3 to 120 ± 4 nm/turn. For dsRNA, the effects of $CoHex^{3+}$ on $\Delta\sigma$ and δ are more significant at 10 than at 150 mM NaCl, which may be due to the competition between Na^+ and $CoHex^{3+}$. We failed to determine the effects of $CoHex^{3+}$ on $\Delta\sigma$ and δ of dsDNA at 10 mM NaCl due to condensation.

Mg^{2+} affects the R-x curves of DNA and RNA in the same direction at 150 mM NaCl [Figs. 3(b) and 3(d)]. We found 100 mM Mg^{2+} overwinds both DNA ($0.92 \pm 0.02\%$) and RNA ($3.12 \pm 0.10\%$) [Fig. 3(f)], decreases both δ_{DNA} (73 ± 3 to 56 ± 2 nm/turn) and δ_{RNA} (81 ± 4 to 61 ± 2 nm/turn) [Fig. 3(h)].

To explain our experiments of the effects of cations on DNA and RNA, we performed all-atom molecular dynamics (MD) simulations with 4 mM $CoHex^{3+}$ or 100 mM Mg^{2+} at 150 mM NaCl using CGACTCTACGGCATCTGCGC for dsDNA [42] and the same sequence for dsRNA except that T bases were replaced by U in dsRNA. The initial structures of B-DNA and A-RNA were built using the nucleic acid builder of AMBER [43]. Na^+, $CoHex^{3+}$, and Mg^{2+} were described by the ion models used in previous studies [44–46]. The bulk ion concentrations were confirmed before the 500 ns all-atom simulations (Figs. S3–S5 [31]) [2,46]. See the calculations of the structural and elastic parameters in the Supplemental Material (Figs. S6 and S7 and supplemental method [31]) [47,48].

We summarize the effects of $CoHex^{3+}$ and Mg^{2+} on the elasticities of dsDNA and dsRNA at 150 mM NaCl obtained by MT experiments and MD simulations (Table I and Fig. S8 in Ref. [31]). Simulation results for $CoHex^{3+}$ and Mg^{2+} are qualitatively consistent with those obtained by MT experiments. $CoHex^{3+}$ decreases P, K, $\Delta\sigma$, and δ of dsDNA but increases those of dsRNA, slightly shortens L_{DNA}, whereas significantly shortens L_{RNA}. Mg^{2+} decreases P, L, and δ while increases $\Delta\sigma$ of both dsDNA and dsRNA, reduces K_{DNA}, but raises K_{RNA}. Thus, for dsDNA and dsRNA, $CoHex^{3+}$ affects P, K, $\Delta\sigma$, and δ oppositely whereas Mg^{2+} only affects K oppositely.

As shown in Fig. 4 and Table II, our simulations reveal that $CoHex^{3+}$ mainly binds to the phosphates of B-DNA whereas it mainly binds to the deeper and narrower major groove of A-RNA, which is consistent with previous simulations [2,5,6]. Our simulations were performed at mM concentrations of $CoHex^{3+}$ and physiological concentrations of NaCl, similar to previous studies [6]. The ways we calculated P and L are also the same as previous studies [6]. Thus, we obtained similar elastic parameters (Table S1 [31]). Different from $CoHex^{3+}$, Mg^{2+} mostly prefers the major grooves of both dsDNA and dsRNA, which agrees with previous simulations [46]. See the calculation of the distributions of $CoHex^{3+}$ and Mg^{2+} in the Supplemental Material (Fig. S9 and supplemental method [31]).

As shown in Fig. 4 and Table III, $CoHex^{3+}$ and Mg^{2+} remarkably alter the structure of dsRNA while $CoHex^{3+}$ moderately alters the structure of dsDNA. $CoHex^{3+}$ dramatically narrows down the major groove width of dsRNA from 0.69 ± 0.17 to 0.20 ± 0.02 nm. The very small fluctuation of the major groove width of dsRNA (± 0.02 nm) suggests that $CoHex^{3+}$ is tightly clamped in the major groove of dsRNA. Weaker than the effect of $CoHex^{3+}$,

TABLE I. Effects of $CoHex^{3+}$ and Mg^{2+} on the elasticities of dsDNA and dsRNA revealed by MT experiments and MD simulations at 150 mM NaCl. The averages of P, K, L, $\Delta\sigma$, $\Delta\Pi$, and δ without multivalent cations and at the maximum determined concentrations are listed. $\Delta\Pi$ is the modification of helical pitch caused by binding of $CoHex^{3+}$ or Mg^{2+}, which is calculated based on $\Delta\sigma$. The positive and negative effects are marked with "↑"and "↓", respectively.

	$CoHex^{3+}$ (MT)		$CoHex^{3+}$ (MD)	
	DNA	RNA	DNA	RNA
	0–100 mM		0–4 mM	
P (nm)	46 ↓ 43	57 ↓ 79	51 ↓ 40	57 ↑ 97
K (pN)	1331 ↓ 1231	564 ↑ 821	1473 ↓ 1392	467 ↑ 907
L (nm/bp)	0.340 ↓ 0.336	0.280 ↓ 0.265	0.333 ↓ 0.331	0.279 ↓ 0.248
	0–1 mM		0–4 mM	
$\Delta\sigma$ (%)	−0.32↓	3.66↑	−0.8↓	3.9↑
$\Delta\Pi$ (bp/turn)	−0.03↓	0.40↑	−0.08↓	0.43↑
δ (nm)	73 ↓ 63	81 ↑ 98	not available	

	Mg^{2+} (MT) 0–100 mM		Mg^{2+} (MD) 0–100 mM	
	DNA	RNA	DNA	RNA
P (nm)	46 ↓ 43	57 ↓ 47	51 ↓ 48	57 ↓ 54
K (pN)	1330 ↓ 1130	564 ↓ 690	1473 ↓ 1336	467 ↑ 619
L (nm/bp)	0.341 ↓ 0.331	0.279 ↓ 0.265	0.333 ↓ 0.330	0.279 ↓ 0.263
$\Delta\sigma$ (%)	0.92↑	3.12↑	0.29↑	2.13↑
$\Delta\Pi$ (bp/turn)	0.10↑	0.34↑	0.03↑	0.23↑
δ (nm)	73 ↓ 56	81 ↓ 61	not available	

Mg^{2+} narrows down the major groove width of dsRNA from 0.69 ± 0.17 to 0.39 ± 0.10 nm. The normal fluctuation of the major groove width of dsRNA (± 0.10 nm) suggests that Mg^{2+} is not tightly clamped. For dsDNA, Mg^{2+} has no obvious effect on the grooves whereas $CoHex^{3+}$ moderately narrows down the minor groove width from 0.57 ± 0.05 to 0.47 ± 0.05 nm.

In the absence of multivalent cations, the major groove width of dsRNA has a significant larger fluctuation (± 0.17 nm) than the fluctuations (± 0.02 to ± 0.06 nm) of other groove widths (the major and minor grooves of

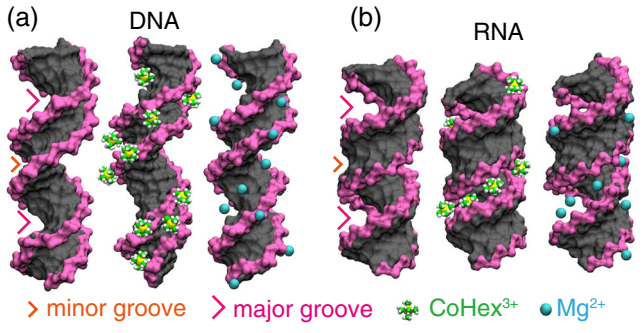

FIG. 4. Representative structures of dsDNA and dsRNA showing the binding of $CoHex^{3+}$ and Mg^{2+} revealed by MD simulations.

TABLE II. Distributions of $CoHex^{3+}$ and Mg^{2+} on dsDNA and dsRNA revealed by MD simulations.

	Phosphates	Major groove	Minor groove
$CoHex^{3+}$ on DNA	57%	29%	14%
$CoHex^{3+}$ on RNA	12%	72%	16%
Mg^{2+} on DNA	30%	49%	21%
Mg^{2+} on RNA	15%	61%	24%

TABLE III. Effects of $CoHex^{3+}$ and Mg^{2+} on the groove sizes of dsDNA and dsRNA at 150 mM NaCl revealed by MD simulations. The averages and standard deviations of the width and depth of the grooves are listed for comparison.

Width/depth in nm	DNA	DNA at $CoHex^{3+}$	DNA at Mg^{2+}
Major groove width	1.19 ± 0.06	1.22 ± 0.06	1.18 ± 0.07
Minor groove width	0.57 ± 0.05	0.47 ± 0.05	0.58 ± 0.05
Major groove depth	0.53 ± 0.07	0.51 ± 0.07	0.56 ± 0.08
Minor groove depth	0.49 ± 0.03	0.51 ± 0.03	0.48 ± 0.03
	RNA	RNA at $CoHex^{3+}$	RNA at Mg^{2+}
Major groove width	0.69 ± 0.17	0.20 ± 0.02	0.39 ± 0.10
Minor groove width	0.98 ± 0.02	1.02 ± 0.02	1.01 ± 0.02
Major groove depth	1.04 ± 0.05	0.99 ± 0.02	1.02 ± 0.04
Minor groove depth	0.11 ± 0.02	0.08 ± 0.01	0.10 ± 0.02

dsDNA as well as the minor groove of dsRNA). This interesting finding is consistent with previous simulation results of other DNA and RNA sequences [48,49]. See the calculation of the groove sizes and the comparisons with previous simulations in the Supplemental Material (Figs. S10 and S11 and supplemental method [31]).

The distinct effects of $CoHex^{3+}$ on the elastic parameters of dsDNA and dsRNA can be attributed to its different binding modes on dsDNA and dsRNA. The binding of $CoHex^{3+}$ at the major groove of dsRNA causes the contraction along its helical axis and dramatically narrows down its major groove (Table III). Thus $CoHex^{3+}$ is tightly clamped in the major groove and further bending of dsRNA becomes energetically more expensive, which stiffens dsRNA [6]. When $CoHex^{3+}$ binds to dsDNA, the increased bending flexibility (i.e., reduced persistence length) of dsDNA can be attributed to the neutralization of the highly negatively charged backbone [6]. For the contour length, because $CoHex^{3+}$ dramatically narrows down the major groove of dsRNA whereas it only moderately narrows down the minor groove of dsDNA, $CoHex^{3+}$ shortens the contour length of dsRNA more significantly than dsDNA.

In the term of the effect on the elasticities of dsRNA, $CoHex^{3+}$ stiffens dsRNA but Mg^{2+} softens dsRNA in bending [Figs. 2(c) and 2(d) and Table I]. When a sort of cation binds to dsDNA and dsRNA, it typically neutralizes the backbone anyway, lowering down the persistence length, unless there is sufficient narrowing of the major groove that can outweigh the effect of charge neutralization and increase the persistence length. $CoHex^{3+}$ mainly binds into the major groove of dsRNA and significantly narrows it down. Thus, $CoHex^{3+}$ is tightly clamped, which stiffens dsRNA. Mg^{2+} prefers the major groove of dsRNA [Fig. 4(b) and Table II] but does not narrow down the major groove sufficiently to tightly clamp Mg^{2+} (Table III). Mg^{2+} neutralizes the negatively charged backbone of dsRNA and slightly softens dsRNA, in analogy to dsDNA.

It is worth highlighting that the dsRNA is significantly overwound (the modification of helical pitch, $\Delta\Pi \sim 0.40$ bp/turn at 1 mM $CoHex^{3+}$ and 150 mM NaCl) and shortened by $CoHex^{3+}$. In the absence of high-valent cations, the helical density of the *A*-form RNA is lower than the *B*-form DNA. However, in the presence of high-valent cations, dsRNA can become even more twisted than dsDNA. As the helical densities and the structures of dsDNA and dsRNA are altered by high-valent cations under physiological monosalt concentration, the interactions of the duplexes with proteins and other binding ligands may be regulated by high-valent cations *in vivo*.

We are grateful for the financial support from National Natural Science Foundation of China (No. 31670760, No. 11704286, and No. 11575128), the valuable discussions with Professor John Marko, Professor Xiangyun Qiu, and Professor Shiyong Ran, and the Super Computing Center of Wuhan University.

*H. F., C. Z., and X.-W. Q. contributed equally to this work.
†Corresponding author.
zhxh@whu.edu.cn
‡Corresponding author.
zjtan@whu.edu.cn

[1] L. Li, S. A. Pabit, S. P. Meisburger, and L. Pollack, Phys. Rev. Lett. **106**, 108101 (2011).
[2] Y. Y. Wu, Z. L. Zhang, J. S. Zhang, X. L. Zhu, and Z. J. Tan, Nucleic Acids Res. **43**, 6156 (2015).
[3] S. A. Pabit, X. Y. Qiu, J. S. Lamb, L. Li, S. P. Meisburger, and L. Pollack, Nucleic Acids Res. **37**, 3887 (2009).
[4] F. Pan, C. Roland, and C. Sagui, Nucleic Acids Res. **42**, 13981 (2014).
[5] I. S. Tolokh, S. A. Pabit, A. M. Katz, Y. Chen, A. Drozdetski, N. Baker, L. Pollack, and A. V. Onufriev, Nucleic Acids Res. **42**, 10823 (2014).
[6] A. V. Drozdetski, I. S. Tolokh, L. Pollack, N. Baker, and A. V. Onufriev, Phys. Rev. Lett. **117**, 028101 (2016).
[7] S. B. Smith, Y. J. Cui, and C. Bustamante, Science **271**, 795 (1996).
[8] G. S. Manning, Biophys. J. **91**, 3607 (2006).
[9] A. V. Dobrynin, Macromolecules **39**, 9519 (2006).

[10] A. Brunet, C. Tardin, L. Salome, P. Rousseau, N. Destainville, and M. Manghi, Macromolecules **48**, 3641 (2015).
[11] J. A. Abels, F. Moreno-Herrero, T. van der Heijden, C. Dekker, and N. H. Dekker, Biophys. J. **88**, 2737 (2005).
[12] E. Herrero-Galan, M. E. Fuentes-Perez, C. Carrasco, J. M. Valpuesta, J. L. Carrascosa, F. Moreno-Herrero, and J. R. Arias-Gonzalez, J. Am. Chem. Soc. **135**, 122 (2013).
[13] J. Lipfert *et al.*, Proc. Natl. Acad. Sci. U.S.A. **111**, 15408 (2014).
[14] C. Zhang, H. Fu, Y. J. Yang, E. C. Zhou, Z. J. Tan, H. J. You, and X. H. Zhang, Biophys. J. **116**, 196 (2019).
[15] S. Guilbaud, L. Salome, N. Destainville, M. Manghi, and C. Tardin, Phys. Rev. Lett. **122**, 028102 (2019).
[16] C. G. Baumann, S. B. Smith, V. A. Bloomfield, and C. Bustamante, Proc. Natl. Acad. Sci. U.S.A. **94**, 6185 (1997).
[17] M. D. Wang, H. Yin, R. Landick, J. Gelles, and S. M. Block, Biophys. J. **72**, 1335 (1997).
[18] C. G. Baumann, V. A. Bloomfield, S. B. Smith, C. Bustamante, M. D. Wang, and S. M. Block, Biophys. J. **78**, 1965 (2000).
[19] L. R. Brewer, M. Corzett, and R. Balhorn, Science **286**, 120 (1999).
[20] X. Zhuang, Science **305**, 188 (2004).
[21] W. B. Fu, X. L. Wang, X. H. Zhang, S. Y. Ran, J. Yan, and M. Li, J. Am. Chem. Soc. **128**, 15040 (2006).
[22] F. Ritort, S. Mihardja, S. B. Smith, and C. Bustamante, Phys. Rev. Lett. **96**, 118301 (2006).
[23] S. Husale, W. Grange, M. Karle, S. Burgi, and M. Hegner, Nucleic Acids Res. **36**, 1443 (2008).
[24] X. L. Wang, X. H. Zhang, M. W. Cao, H. Z. Zheng, B. Xiao, Y. L. Wang, and M. Li, J. Phys. Chem. B **113**, 2328 (2009).
[25] K. Besteman, K. Van Eijk, and S. G. Lemay, Nat. Phys. **3**, 641 (2007).
[26] K. Besteman, S. Hage, N. H. Dekker, and S. G. Lemay, Phys. Rev. Lett. **98**, 058103 (2007).
[27] B. A. Todd and D. C. Rau, Nucleic Acids Res. **36**, 501 (2008).
[28] K. T. Liu and S. Y. Ran, Phys. Chem. Chem. Phys. **21**, 2919 (2019).
[29] Z. Guo, Y. Wang, A. Yang, and G. Yang, Soft Matter **12**, 6669 (2016).
[30] Y. J. Yang, L. Song, X. C. Zhao, C. Zhang, W. Q. Wu, H. J. You, H. Fu, E. C. Zhou, and X. H. Zhang, ACS Synth. Biol. **8**, 1663 (2019).
[31] See Supplemental Material at http://link.aps.org/supplemental/10.1103/PhysRevLett.124.058101 for detailed protocols to prepare the torsion-constrained DNA and RNA duplexes and the detailed methods of the simulations, which includes Refs. [32–34].
[32] D. M. York, T. A. Darden, and L. G. Pedersen, J. Chem. Phys. **99**, 8345 (1993).
[33] S. Miyamoto and P. A. Kollman, J. Comput. Chem. **13**, 952 (1992).
[34] R. Lavery, M. Moakher, J. H. Maddocks, D. Petkeviciute, and K. Zakrzewska, Nucleic Acids Res. **37**, 5917 (2009).
[35] D. H. Paik, V. A. Roskens, and T. T. Perkins, Nucleic Acids Res. **41**, e179 (2013).
[36] X. H. Zhang, Y. Y. Qu, H. Chen, I. Rouzina, S. L. Zhang, P. S. Doyle, and J. Yan, J. Am. Chem. Soc. **136**, 16073 (2014).
[37] X. H. Zhang, H. Chen, S. M. Le, I. Rouzina, P. S. Doyle, and J. Yan, Proc. Natl. Acad. Sci. U.S.A. **110**, 3865 (2013).
[38] X. H. Zhang, H. Chen, H. X. Fu, P. S. Doyle, and J. Yan, Proc. Natl. Acad. Sci. U.S.A. **109**, 8103 (2012).
[39] T. Odijk, Macromolecules **28**, 7016 (1995).
[40] T. R. Strick, J. F. Allemand, D. Bensimon, and V. Croquette, Biophys. J. **74**, 2016 (1998).
[41] J. D. Moroz and P. Nelson, Proc. Natl. Acad. Sci. U.S.A. **94**, 14418 (1997).
[42] R. S. Mathew-Fenn, R. Das, and P. A. B. Harbury, Science **322**, 446 (2008).
[43] A. Perez, I. Marchan, D. Svozil, J. Sponer, T. E. Cheatham, 3rd, C. A. Laughton and M. Orozco, Biophys. J. **92**, 3817 (2007).
[44] I. S. Joung and T. E. Cheatham III, J. Phys. Chem. B **112**, 9020 (2008).
[45] T. D. Sun, A. Mirzoev, N. Korolev, A. P. Lyubartsev, and L. Nordenskiold, J. Phys. Chem. B **121**, 7761 (2017).
[46] K. Xi, F. H. Wang, G. Xiong, Z. L. Zhang, and Z. J. Tan, Biophys. J. **114**, 1776 (2018).
[47] L. Bao, X. Zhang, Y. Z. Shi, Y. Y. Wu, and Z. J. Tan, Biophys. J. **112**, 1094 (2017).
[48] J. H. Liu, K. Xi, X. Zhang, L. Bao, X. H. Zhang, and Z. J. Tan, Biophys. J. **117**, 74 (2019).
[49] K. Liebl, T. Drsata, F. Lankas, J. Lipfert, and M. Zacharias, Nucleic Acids Res. **43**, 10143 (2015).